MANUSCRIPT TITLE:

Biochemical characterizations of Pontocerebellar Hypoplasia linked mutations of Target of Egr1 (TOE1) reveal impacts on thermal stability, ribonuclease activity, and oligomerization.

AUTHORS

Lizette Zavala[1], Magdalena Sobien[1,2,3], and Cassandra K. Hayne[1,4,5,] *

[1] Department of Biochemistry and Molecular Biology, University of Chicago, Chicago, Illinois, 60637, USA

[2] Laboratory of Neurobiology, Nencki Institute of Experimental Biology BRAINCITY, Warsaw, 02093, Poland

[3] Faculty of Breeding, Bioengineering and Animal Protection, Warsaw University of Life Sciences, Warsaw, 02786, Poland

[4] Neuroscience Institute, University of Chicago, Chicago, Illinois, 60637, USA

[5] Institute for Biophysical Dynamics, University of Chicago, Chicago, Illinois, 60637, USA

* To whom correspondence should be addressed. Tel: 1-773-702-9078; Email: chayne@uchicago.edu

Present Address: Magdalena Sobien, Laboratory of Neurobiology, Nencki Institute of Experimental Biology BRAINCITY, Warsaw, 02093, Poland

ABSTRACT

The Target of EGR1 (TOE1) gene encodes the TOE1 deadenylase, which is essential for the maturation of Pol-II transcribed snRNAs in humans. Over a dozen missense mutations in the TOE1 gene have been linked to Pontocerebellar Hypoplasia Type 7 (PCH7), a rare but serious neurodevelopmental and neurodegenerative disease that leads to early mortality. The biochemical mechanisms for why these PCH7-linked mutations alter TOE1's biochemical characteristics remains vague. Here, we utilized AlphaFold predicted structures of TOE1 and biochemical characterizations to investigate the impact of TOE1 variants on TOE1's biochemical properties.

We performed characterization of the thermal stability and activity of eleven PCH-linked TOE1 variants and found that eight variants have significant reduced protein thermal

stability and only two variants impair TOE1's ribonuclease activity, particularly its exonuclease activity. Additionally, we found that the F148Y mutation impacts TOE1's oligomeric state *in vitro* and *in vivo*. Together, these results demonstrated that PCH-linked mutations of TOE1 impact many different aspects of TOE1 biochemistry, providing novel insights which may provide potential therapeutic strategies to treat PCH7 patients. In addition, these mutations provide a library of TOE1 variants that will be useful for future studies of TOE1 function and regulation.

INTRODUCTION

Deadenylases play critical cellular roles in regulating the maturation and degradation of mRNAs and many non-coding RNAs (ncRNAs) through the cleavage of RNA poly(A) tails. Processing of RNAs by deadenylases is important for the stabilization, degradation, regulation, and/or function of the RNA substrate(1–5). Currently, there are three known human ncRNA deadenylases: poly(A) specific ribonuclease (PARN), U6 snRNA phosphodiesterase 1 (USB1), and Target of Egr1 (TOE1)(6). TOE1 is a unique and essential enzyme capable of both deadenylase (removal of Poly(A)'s) and 3'-to-5' exonuclease activity. The cellular role of TOE1 is to remove the 3'-post-transcriptionally added poly(A) tails of small ncRNAs during their maturation(6–12), and to protect these RNA substrates from early degradation and processing(6, 13). Although many ncRNA substrates are shared among TOE1 and PARN, TOE1 is the deadenylase responsible for targeting Pol-II transcribed small nuclear RNA (snRNA) precursors(6–12). Evidence of a defect in snRNA processing due to loss of TOE1 was shown by a rescue experiment utilizing a catalytically inactive mutant and wildtype TOE1. The study also revealed that PCH patient derived fibroblasts (E220K, F148Y, and A103T) had a defect in snRNA processing(7).

Pontocerebellar hypoplasia (PCH) is an autosomal recessive pediatric neurodevelopmental and neurodegenerative disease classified based on genotype and phenotype(8). Biallelic (homozygous) and compound heterozygous mutations of TOE1 are linked to (PCH7) (7, 14–18). Hallmarks of PCH7 are similar to other PCH subtypes: atrophy of the pons and cerebellum, breathing abnormalities, and muscular hypotonia; however, PCH7 also includes a unique phenotype of hypogonadism(7, 8). The mechanism by which mutations in TOE1 lead to PCH7 remain poorly understood. Similarly, little is known about how TOE1 recognizes its preferred RNA substrates, or how it is regulated.

PCH7-linked mutations occur throughout the TOE1 protein and have been linked to decreased protein levels and changes in cellular localization(7, 17), which suggests that mutations could impact different aspects of TOE1 function and regulation. Presently, no robust biochemical analysis of these mutations has been performed. Here, we utilize AlphaFold predictions and biochemical assays to better understand how PCH7-linked mutations impact TOE1 function *in vitro* towards an understanding of how they impact TOE1 cellular functions. We further extrapolate what we learned from this set of mutants to provide novel insights into TOE1's biochemical properties.

MATERIAL AND METHODS

Cloning and generation of plasmids

A codon-optimized gene for TOE1 and all variants was generated by Genscript. TOE1 was subcloned into the pHis2-parallel vector with an N-terminal His tag using BamHI and XhoI sites and into pCDNA3.1 vectors (with N-terminal HA, GFP, and Flag tags) using KpnI, BamHI, and HindIII sites, using standard protocols. Cloning into pCDNA vectors was performed both in house and by Genscript. A table of plasmids used in this work can be found in Supplemental Table 1.

Recombinant expression and purification of TOE1 from *E.Coli*

His-TOE1 was expressed in BL21(DE3) Rosetta II pLac(I) cells (Millipore). Cells were grown at 37°C to an optical density of 0.4-0.6, in LB, and protein production was induced by the addition of 0.1 mM IPTG at 18°C, overnight. Cells were harvested and pellets were stored at -80°C until purification. Cells were lysed via sonication in 50 mM HEPES pH 8.0, 750 mM NaCl, 10% glycerol, 5 mM $MgCl_2$, 10 mM imidazole, and 5 mM BME, with the addition of a Complete EDTA-free protease inhibitor tablet (Roche). Purification was conducted using HIS-60 resin (Takara). Resin was washed first with lysis buffer and then washed with 50 mM HEPES pH 8.0, 250 mM NaCl, 10% glycerol, 5 mM $MgCl_2$, 10 mM imidazole, 5 mM BME. The sample was eluted in the same buffer, with the addition of 250 mM Imidazole. Protein eluate was then loaded onto a HiTrap™ Heparin HP (Cytiva), equilibrated with 50 mM HEPES pH 8.0, 250 mM NaCl, 10% glycerol, 5 mM $MgCl_2$ and 1 mM DTT and eluted at approximately 750

mM NaCl, over a salt gradient. The final protein concentration was measured using a NanoDrop^{C} (Thermo Scientific).

Differential Scanning Fluorimetry (DSF)

DSF assays were performed using protein eluted from the heparin column within 24 hours of purification, without concentration. Assays were performed with 1.95 µM TOE1 in 750 mM NaCl, 50 mM HEPES, 10% Glycerol, 5 $MgCl_2$, and 2X SYPRO Orange (Invitrogen). Each experimental measurement was collected and averaged from technical replicates, in which each reported melt temperature was recorded from independent protein purifications, and experimental replicates were performed on different days. TOE1 thermal stability was measured from 4 to 95°C, with 1°C/minute ramp rate on a CFX96 (Bio-Rad) using the CFX Manager 3.1. First derivative curves were obtained, confirmed to be one state, and fit to a Gaussian in GraphPad Prism version 10 to determine the melt temperature. Statistical analysis was performed using a One-Way Anova in GraphPad Prism version 10.

TOE1 ribonuclease assays

Ribonuclease assays were performed at 37°C in 26 mM HEPES pH 8.0, 150 mM NaCl, 2.6 mM $MgCl_2$, 2% glycerol, 0.4 mM DTT, 0.8 mM Spermidine, 0.08 mg/ml bovine serum albumin, 0.8% IPGAL CA-630 (Sigma Aldrich), and murine RNase inhibitor (NEB, diluted 10,000X) with 500 nM 5'-flourescein labelled RNA substrate and 250 nM TOE1. Each set of assays included TOE1^{WT} as a positive control and TOE1^{D64A,E66A} as a negative control for ribonuclease contamination. Timepoints were quenched with loading dye containing UREA. Samples were separated by electrophoresis on 15% TBE-Urea gels (Invitrogen) for 60 min at 180 V and then imaged using a ChemiDocMP (Bio-Rad). Analysis of TOE1 cleavage was performed using ImageJ. For the analysis, the RNA amounts across different regions of the gel were quantified, using the RNA ladder to determine product states. Total RNA across all regions was calculated with the bottom of the 20 nucleotide band used as the cut-off for what had not been fully deadenylated and the top of the 2 nucleotide band used to calculate the RNA that had completed cleavage.

Structural predictions

Structural predictions were performed using AlphaFold 3(19), using WT TOE1 as the input sequence.

Immunoprecipitation of TOE1^{F148Y} and TOE1^{WT} from HEK293T cells

HEK293T cells were obtained from ATCC and cultured in high glucose Dulbecco's Modified Eagle Medium (DMEM, Gibco) and supplemented with 1 mM sodium pyruvate, 50 units/mL penicillin/streptomycin solution (Gibco), and 10% fetal bovine serum (FBS, Cytiva). HEK293T cells were transfected with plasmid DNA, using FuGENE HD. Cells were harvested and washed with Phosphate-Buffered Saline (PBS). Cells were lysed with a buffer composed of 50 mM HEPES, pH 8.0, 5 mM $MgCl_2$, 200 mM NaCl, 10% glycerol, 0.05% IGEPAL CA-630 (Sigma Aldrich), 2 mM Phenylmethylsulfonyl fluoride (PMSF). Clarified cell lysates were incubated with Anti-HA agarose resin (Genscript) and then washed with the lysis buffer before the resin was boiled in loading dye. Western blots were performed using standard protocols. The antibodies used were: anti-MYC tag antibody (Clone 4A6, Millipore) and anti-HA (C29F4, Cell Signalling Technology). Samples were analyzed by quantifying the adjusted volume of the bands, using Image Lab (Bio-Rad). Then, the ratio of adjusted volumes for bait/prey were calculated and compared as a fraction of the wildtype bait/wildtype prey. Statistical significance was calculated using a One-Way Anova.

Size exclusion chromatography

TOE1 samples were separated on a Superdex 200 Increase (Cytiva) equilibrated with 50 mM HEPES, pH 8.0, 250 mM NaCl, 2% glycerol, 5 mM $MgCl_2$, and 1 mM DTT. Assays on peak fractions were performed as described above.

RESULTS

Architecture of TOE1 and PCH variants utilized in our studies.

To study the impact of PCH mutations on the biochemical properties of TOE1, we first selected eleven established PCH-linked missense mutations in TOE1(7, 15), located throughout the protein (Figure 1A). As a monomer, TOE1 is a 56.5 kDa protein with three main domains: the DEDD-type deadenylase domain, a C3H zinc finger, and a nuclear localization signal (NLS)(11, 20, 21). The selected mutations occur throughout TOE1 but are more frequently found within the deadenylase domain.

We then utilized AlphaFold3(19) to predict the structure of TOE1 and reveal the potential molecular environments in which these PCH variants occur (Figure 1B). The structure reveals a globular deadenylase domain, which contains the catalytic core. The deadenylase domain is connected to the C3H zinc finger, which forms the base of a helix containing the NLS. In addition to these central ordered domains, there is a loop and the C-terminal tail, which are both unstructured. Most of the PCH-linked variants are found within the deadenylase domain with some scattered near or within the zinc finger domain (Figure 1A,B). Notably, while S496 is not within the previously defined boundaries of the deadenylase domain of TOE1 (Figure 1A), in the AlphaFold structure (Figure 1B), there are two alpha-helices and three beta-strands (which appear to extend an existing beta-sheet) that contribute to the structure of the deadenylase domain (shown in grey), and S496 resides in one of these helices. No mutations were located within the active site, the NLS, nor in the major disordered regions.

In addition, because cellular deadenylases frequently function as homo and heterodimers(6, 13, 22), we also used AlphaFold 3(19) to predict the homodimerization of TOE1. The predicted TOE1 homodimer structure revealed that F148 appears at the dimer interface (Figure 1C), suggesting that this mutation could disrupt homodimerization.

Purification of active recombinant TOE1 variants to high purity.

To begin studying TOE1 biochemically, we expressed TOE1 variants in *E.coli* and performed affinity purification using an encoded N-terminal His-tag, similar to previous studies(13). We then performed an additional purification using heparin affinity chromatography, which generated a concentrated fraction of TOE1 for further study (Supplemental Figure 1). To confirm that the purity of this workflow resulted in protein free from substantial ribonuclease contamination, we tested the activity of $TOE1^{WT}$ and a

previously reported catalytic-deficient variant (TOE1$^{D64A, E66A}$)(13). For these assays, we utilized a previously reported stem-loop containing deadenylase substrate(23), which contains a stem-loop with alternating weak (A:U) and strong (C:G) base pairs, an AAAU, and then a 3' poly(A) tail (Figure 2A). Use of this substrate allowed us to observe both the deadenylase and exonuclease activities of TOE1^{WT}, which are absent in the catalytic-deficient TOE1$^{D64A, E66A}$ sample (Figure 2B).

PCH-linked variants can impact TOE1 deadenylase activity.

We then utilized our ribonuclease assay to assess how PCH-linked variants could alter TOE1 activity *in vitro*. Each PCH-linked TOE1 variant was assayed for deadenylase and exonuclease activity across a time course (Figure 3). Under our assay conditions, we reproducibly saw that TOE1^{WT} would deadenylate most of the 20-nucleotide poly(A) tail of its RNA substrate in 5 minutes, with almost complete deadenylation in 10 minutes (Figure 2B, Figure 3A). We thus used the 10-minute timepoint to compare deadenylation completion across PCH variants. We consistently observed mild differences in deadenylase activity for TOE1^{R73S}, TOE1^{A103T}, and TOE1^{F148Y}, with only TOE1^{F148Y} having a statistically significant difference in cleavage (Figure 3B,C,D, M, Supplemental Table 2). These three amino acids, along with V173, are located near the active site (Figure 4A).

PCH-linked variants frequently impact TOE1 exonuclease activity.

Using these assays, we also examined TOE1's exonuclease activity by observing how TOE1 cleaved the RNA substrate following deadenylation. Because wildtype TOE1 typically finished cleaving the RNA by the 30-minute timepoint (Figure 2B, Figure 3A), we selected the 30-minute and 60-minute timepoints to compare variants (Figure 3N,O). From these data, we observed that, in contrast to the deadenylase activity, only two mutants had exonuclease profiles similar to TOE1^{WT}: TOE1^{E220K} and TOE1^{S496F} (Figure 3F,L,N). When we examined the location of these two mutations, we observed that they are in the same region of TOE1, connecting a C-terminal alpha helix to the deadenylase domain of TOE1 (Figure 4B), suggesting this region is not important for catalytic function but has another important role in TOE1 function or regulation.

All other mutants had impaired exonuclease activity, compared with TOE1^{WT}, over the time-course, under these assay conditions (Figure 3N,O). Interestingly, we observed an intermediate impact on exonuclease activity by the H319 variants. TOE1^{H319Q} and TOE1^{H319Y}

generally approached completion over the time course of our assays (Figure 3J,K,N,O), albeit at a slower pace than TOE1^{WT}, TOE1^{E220K}, or TOE1^{S496F}. TOE1$^{H319Q/Y}$ had statistically significant differences in completion, compared with TOE1^{WT}, at 30 minutes, but not 60 minutes (Figure 3N,O). H319 lies within the zinc finger domain. When we examined the sequence and structure of the zinc finger, we saw that there are two histidine residues within the C3H zinc finger domain, H295 and H319. However, our structure suggested that H319 is best positioned to form the zinc binding pocket with the cysteines. Therefore, we used AlphaFold to model zinc into the TOE1 structure. AlphaFold placed the zinc ion within the zinc finger, with the zinc being coordinated by H319, C300, C309, and C315 (Figure 4C). This strongly suggests that H319 is the functional C3H zinc finger histidine. Zinc fingers can play important roles in recognizing and binding to RNA substrates based on their sequence, secondary structure, or negatively charged backbone(24, 25). Thus, we hypothesize that the intermediate reduction in exonuclease activity we observed for these zinc finger mutants could be related to something about RNA recognition, specifically after deadenylation.

PCH mutations can impact the thermal stability of TOE1.

Previous studies of other PCH-linked RNA processing enzymes, the RNA exosome(18, 27–31) and tRNA splicing endonuclease complex(32) reveal a reduction in thermal stability for PCH mutations tested, suggesting reduced protein stability may be characteristic of PCH mutations. We thus reasoned that the reduced ribonuclease activity we observed in our ribonuclease assays could be due to reduced stability of TOE1. Therefore, we tested the thermal stability of TOE1 *in vitro,* using differential scanning fluorimetry (DSF). Thermal stability analysis revealed that TOE1^{WT} had a melting temperature (T_m) of 53.54 °C ± 0.70 and catalytically inactive TOE1 had a T_m of 57.11 °C ± 0.32 ($p < 0.0001$) (Figure 5A). Analysis of our eleven PCH-linked variants revealed that eight mutants (TOE1^{A103T}, TOE1^{F148Y}, TOE1^{V173G}, TOE1^{E220K}, TOE1^{F239S}, TOE1^{H319Q}, TOE1^{H319Y}, and TOE1^{S496F}) had statistically significantly lower thermal stabilities than WT, although all remain above physiological temperature. We observed the most severe reduction in T_m for TOE1^{A103T}, TOE1^{F148Y}, and TOE1^{V173G}, which are all in regions that are near the active site and appear to be in regions important for TOE1 stability (Figure 5 B,C). We also found that three PCH-linked variants (TOE1^{R73S}, TOE1^{R253W}, and TOE1^{S304L}) did not have a thermal stability that was significantly different from TOE1^{WT} (Figure 5A, Supplemental Table 3), despite each of the three having reduced ribonuclease

activities. Inspection of these three amino acids revealed that R73 is solvent exposed, near the active site (Figure 5D), while S304 and R253 appear to be important for stabilizing the helix containing the NLS (Figure 5E). Together, these results demonstrate that many, but not all TOE1-linked PCH mutations can impact the thermal stability of TOE1, and that thermal stability may not be the only cause of reduced ribonuclease activity.

TOE1 F148Y has reduced oligomerization.

Finally, we wanted to test the hypothesis that the F148Y mutation could disrupt a TOE1 homodimer. Because the oligomeric state of TOE1 has not been shown biochemically, we utilized a two-prong approach to test if TOE1 forms a homo-oligomer both *in vitro* and *in vivo*. To test if TOE1 forms a homo-oligomer *in vivo* and to assess the impact of TOE1^{F148Y}, we performed TOE1 overexpression and immunoprecipitation experiments in which we co-expressed HA and MYC tagged variants of TOE1^{WT} and TOE1^{F148Y} in HEK293T cells. In these experiments, we co-transfected different combinations of "bait" HA-tagged versions of TOE1 (TOE1^{WT} or TOE1^{F148Y}) and "prey" MYC-tagged TOE1 (TOE1^{WT} or TOE1^{F148Y}). The samples were immunoprecipitated using anti-HA agarose resin to test for the interaction of HA-tagged TOE1 with either TOE1^{WT} or TOE1^{F148Y} MYC-tagged TOE1 variants. We observed the strongest interaction for TOE1^{WT} with itself (Figure 6A, lane 4 compared with lanes 2,3,5, Figure 6B) and observed reduced binding for TOE1^{F148Y}/TOE1^{WT} combinations (Figure 6A, lane 2 and 3 compared with lane 4, Figure 6B). An immunoprecipitation of TOE1^{F148Y} with itself showed consistently reduced interactions (Figure 6A, lane 5 compared to lanes 2-4, Figure 6B). This data supports the idea that TOE1 forms a higher order oligomer *in vivo* and that the TOE1^{F148Y} mutation can disrupt this oligomerization.

To test TOE1 oligomerization by another method, we utilized size-exclusion chromatography and found that TOE1^{F148Y} elutes later than TOE1^{WT} (Figure 6C). Based on the calibration of our column, we calculated an approximate size for TOE1^{WT} at 132.8 ± 3.3 kDa (Figure 6D) which suggests that TOE1 is forming a homodimer, while the molecular weight of TOE1^{F148Y}'s elution volume, 77.8 ± 2.1 kDa, aligns with a TOE1 monomer.

We also tested all the other TOE1 variants, at least once, and did not observe any other variant that impacted TOE1's oligomeric state on the sizing column (Supplemental Figure 2). We confirmed the activity for TOE1 in each peak eluate fraction of TOE1^{WT} and TOE1^{F148Y} (Supplemental Figure 3A,B) and for the other TOE1 variants (N≥1). We observed an

increase in activity after passing each TOE1 variant through the sizing column (Supplemental Figure 3), compared to the heparin samples, in equivalent assay conditions, but the overall trends in ribonuclease activity, compared with $TOE1^{WT}$ did not change.

Therefore, our results suggest that TOE1 forms a homodimer and that $TOE1^{F148Y}$ causes TOE1 to monomerize. Because $TOE1^{F148Y}$ retained activity after the sizing column, we conclude that dimerization is likely not essential for deadenylase activity *in vitro,* although it may still be important for overall function as we observed significant reductions in both deadenylase and exonuclease activities. It is unclear if the reduction we see is due to changes in TOE1 dimerization or other impacts from the F148Y mutation.

DISCUSSION

Our work demonstrates that PCH-linked TOE1 mutations impact a variety of different biochemical properties of TOE1, including the *in vitro* thermal stability, ribonuclease activity of TOE1, and oligomeric state (Figure 7). Importantly, we found that most PCH variants impact the exonuclease activity of TOE1 in a more significant manner, as compared to deadenylase activity, suggesting there could be important distinctions in the substrate specificity of TOE1 RNA processing for patients carrying these mutations. We found that eight PCH variants impact the thermal stability of TOE1 at a statistically significant level and determined that F148Y causes a dramatic shift in TOE1's oligomeric state – from dimer to monomer. The key biochemical findings were strengthened by combining our experimental data with AlphaFold structural predictions to help interpret how the biochemical changes were impacted within the probable molecular environments of these mutations. These various mutations, and their varied impacts on TOE1 function, provide a library from which to better understand the overall function and regulation of TOE1.

This work builds on previous studies which have linked these and other genetic mutations in TOE1 to PCH(7, 14–16, 33). A few studies hint at mechanisms by which mutations may disrupt TOE1 function by examining a single characteristic of TOE1(7, 17); which have typically hinted at differences in protein stability or protein levels. However, no additional formal experimental investigations have been published to characterize how PCH-linked point mutants impact TOE1 function, particularly *in vitro*. In addition, trying to determine how mutations impact TOE1 biology *in vivo* is difficult because only a subset of known mutations have been identified in patients as homozygous mutations (A103T, F148Y,

E220K)(7) while the rest of the patients are compound heterozygotes(7, 14–16, 33). Because PCH is an autosomal recessive disease, each mutation must be causative at some level for patients to have disease. Thus, studying compound heterozygous mutations in patient samples is confounded by the presence of two different mutations; however, the biochemical approaches utilized here provide a framework to decipher the underlying mechanisms by which individual mutations impact TOE1 function.

Furthermore, our approach has allowed us to decipher aspects of TOE1 biology not revealed from studying patient samples alone. For example, for the biallelic mutation, E220K, patient samples revealed a reduction in TOE1 levels(7). Using our approach, we were able to conclude that E220K does not cause a major protein stability defect *in vitro*. Instead, when we examined the molecular environment in which E220 resides, we saw that E220 and S496 appear in a similar region (Figure 4B), and that based on the predicted structure, these two amino acids may form networks that hold a small predicted alpha helix in place. Although we could not clearly decern the importance of this alpha helix, we hypothesize it may be relevant to external interactions for TOE1—such as protein: protein interactions, due to being both surface exposed and away from other key regions (Figure 7). Several previous studies suggest TOE1 interaction partners (7, 11, 13, 20, 34, 35), but the molecular interface where these interactions occur is not known, which is important for validating the specificity of such interactions. As novel TOE1 binding partners are validated, this region should be assessed to see if altering these amino acids can change protein interactions.

From our work, we also speculate that the zinc finger may be involved in RNA recognition and/or specificity. Mutations in and around the zinc finger had either a mild or no impact on TOE1 thermal stability and no obvious impact on deadenylation. However, we found that the zinc finger and zinc finger adjacent mutations all had significant impacts on exonuclease activity. Here, we also proposed that H319 is the key histidine in the C3H zinc finger, and because only a mild impact on thermal stability was found, we believe that the zinc finger is especially important for recognition of non-poly(A) substrates. Currently, how TOE1 recognizes RNA is not known, particularly the difference in how TOE1 recognizes and processes poly(A) and non-poly(A) substrates. Presumably, TOE1 relies on some form of poly(A) tail recognition, as has been identified for other deadenylases(4, 36, 37), but since it is also an exonuclease, how it recognizes diverse substrates is likely more complex. Our work highlights that zinc finger mutations impact deadenylation and exonuclease activity

differently, supporting that there are differences in these modes of TOE1 function, and that some of this recognition may be linked to the zinc finger.

Moreover, previous work on the PAN deadenylase complex has shown that that complex utilizes its zinc finger domain for RNA interactions (24), and we presume TOE1 utilizes its C3H zinc finger in a similar manner. In addition to H319 mutations within the zinc finger, we also found that both TOE1^{S304L} and TOE1^{R253W} had severe impacts on TOE1 exonuclease activity but had no impact on thermal stability (Figure 7). Since both R253 and S304 appear to stabilize the NLS, which is connected to the zinc finger, we hypothesize that these impact zinc finger function as well.

In the absence of an RNA-bound TOE1 structure, further studies will be needed to investigate the role of the zinc finger in TOE1 function. Our work suggests that instead of performing biochemical truncations, which might destabilize a large portion of TOE1, follow-up studies could look at RNA specificity using a TOE1 variant in which the entire C3H motif is mutated. Additionally, further studies are needed to assess if the dimer has a role in RNA recognition and specificity as such a role could explain why the TOE1^{F148Y} mutation had a significant impact on both deadenylation and exonuclease activity, while still maintaining some activity. We believe that the PCH mutations tested here provide a good starting point for further interrogation of the role of the zinc finger in TOE1 RNA substrate recognition.

Another insight gained from combining our structural prediction insights with experimental results was that some PCH-linked mutations, including TOE1^{S304L}, TOE1^{R253W}, and potentially TOE1^{F239S} could impact TOE1 localization (Figure 7). If these mutations were present, we hypothesize that in addition to ribonuclease changes, there could also be a decrease in nuclear localization of TOE1. TOE1 is usually found in the Cajal bodies(17), the sub compartment of the nucleus where most snRNA processing occurs, although there is speculation TOE1 can shuttle between the Cajal bodies and cytoplasm(12,13). Indeed, a recent study showed that a newly identified PCH-linked mutation, the truncated TOE1 variant TOE1^{337*}, causes a slight localization of TOE1 to the cytoplasm when overexpressed(17), while the compound heterozygous mutation it was identified with, TOE1^{F303C}, does not(17). TOE1^{F303C} is located within the zinc finger and can presumably impact ribonuclease activity. The approaches we outlined here could be used in the future to assess novel and addition mutations, such as TOE1^{F303C}.

This work should be interpreted with the obvious limitation that while our *in vitro* studies are able to provide unique insights, they may not fully recapitulate the environment or protein levels of TOE1 in cells, nor the physiological substrates of TOE1, which will carry various modifications. In addition, it is unclear how post-translational modifications could support or alter TOE1 stability *in vivo* or what differences in thermal stability should be considered physiologically relevant. Nevertheless, we believe it would be useful to apply the experimental approaches we optimized here to additional TOE1 variants, to better understand if cellular changes are the result of biochemical properties or some additional feature. Furthermore, we believe the mutations assayed here will be key variants for further investigation of TOE1 function and regulation.

The work presented here contributes to the field by providing the first detailed characterization of PCH mutations, and a biochemical assessment of their impact on TOE1's function. We present the first *in vitro* thermal stability data for TOE1 and have determined conditions compatible with size exclusion chromatography, which were not previously reported, and have allowed us to determine that TOE1 is likely a dimer. These biochemical characterizations provide key biochemical insights and lay an important foundation for future studies and provide the foundation for the development of customized therapeutics targeting specific aspects of TOE1 biology. For example, our findings suggest previously measured reductions in TOE1^{E220K} protein levels may not be due to a thermal stability difference, but rather due to another property, and that TOE1^{F148Y} is a monomer. The results of this work also provide a library of variants that can now be used as controls or point mutations to study different aspects of TOE1 biology, such as differentiating between TOE1 deadenylation and exonuclease activities, understanding the role of the zinc finger, oligomerization, and probing the role of the E220K/S496F region in TOE1: protein interactions.

AUTHOR CONTRIBUTIONS

Lizette Zavala: Conceptualization, Investigation, Formal analysis, Writing – original draft, review & editing, Validation, and Visualization.

Magdalena Sobien: Investigation, Formal analysis, Writing – original draft, review.

Cassandra Hayne: Conceptualization, Formal analysis, Funding acquisition, Methodology, Project Administration, Supervision, Visualization, Writing – original draft, Writing – review & editing.

ACKNOWLEDGEMENTS

We acknowledge Phoebe Rice, Joe Piccirilli, and Viktoriya Kalinina for thoughtful feedback of the manuscript.

FUNDING

This work was supported by the National Institutes of Health / National Institute for General Medical Sciences [R00GM143534 to CKH; LZ was supported by pre-doctoral training fellowships R25GM109439 and T32GM144290]. MS was supported, in part, by the BioLabs Program.

CONFLICT OF INTEREST

The Authors have no conflicts of interest to disclose.

REFERENCES

1. Skeparnias,I., Anastasakis,D., Shaukat,A.-N., Grafanaki,K. and Stathopoulos,C. (2017) Expanding the repertoire of deadenylases. *RNA Biol.*, **14**, 1320–1325.

2. Chen,C.A. and Shyu,A. (2011) Mechanisms of deadenylation-dependent decay. *WIREs RNA*, **2**, 167–183.

3. Nousch,M., Techritz,N., Hampel,D., Millonigg,S. and Eckmann,C.R. (2013) The Ccr4-Not deadenylase complex constitutes the major poly(A) removal activity in *C. elegans*. *J. Cell Sci.*, 10.1242/jcs.132936.

4. Tang,T.T.L., Stowell,J.A.W., Hill,C.H. and Passmore,L.A. (2019) The intrinsic structure of poly(A) RNA determines the specificity of Pan2 and Caf1 deadenylases. *Nat. Struct. Mol. Biol.*, **26**, 433–442.

5. Webster,M.W., Chen,Y.-H., Stowell,J.A.W., Alhusaini,N., Sweet,T., Graveley,B.R., Coller,J. and Passmore,L.A. (2018) mRNA Deadenylation Is Coupled to Translation Rates by the Differential Activities of Ccr4-Not Nucleases. *Mol. Cell*, **70**, 1089-1100.e8.

6. Huynh,T.N. and Parker,R. (2023) The PARN, TOE1, and USB1 RNA deadenylases and their roles in non-coding RNA regulation. *J. Biol. Chem.*, **299**, 105139.

7. Lardelli,R.M., Schaffer,A.E., Eggens,V.R.C., Zaki,M.S., Grainger,S., Sathe,S., Van Nostrand,E.L., Schlachetzki,Z., Rosti,B., Akizu,N., *et al.* (2017) Biallelic mutations in the 3′ exonuclease TOE1 cause pontocerebellar hypoplasia and uncover a role in snRNA processing. *Nat. Genet.*, **49**, 457–464.

8. Van Dijk,T., Baas,F., Barth,P.G. and Poll-The,B.T. (2018) What's new in pontocerebellar hypoplasia? An update on genes and subtypes. *Orphanet J. Rare Dis.*, **13**, 92.

9. Son,A., Park,J.-E. and Kim,V.N. (2018) PARN and TOE1 Constitute a 3′ End Maturation Module for Nuclear Non-coding RNAs. *Cell Rep.*, **23**, 888–898.

10. Lardelli,R.M. and Lykke-Andersen,J. (2020) Competition between maturation and degradation drives human snRNA 3′ end quality control. *Genes Dev.*, **34**, 989–1001.

11. Deng,T., Huang,Y., Weng,K., Lin,S., Li,Y., Shi,G., Chen,Y., Huang,J., Liu,D., Ma,W., *et al.* (2019) TOE1 acts as a 3′ exonuclease for telomerase RNA and regulates telomere maintenance. *Nucleic Acids Res.*, **47**, 391–405.

12. Ma,T., Xiong,E.S., Lardelli,R.M. and Lykke-Andersen,J. (2023) The 3′ exonuclease TOE1 selectively processes snRNAs through recognition of Sm complex assembly and 5′ cap trimethylation. 10.1101/2023.08.15.553431.

13. Wagner,E., Clement,S.L. and Lykke-Andersen,J. (2007) An Unconventional Human Ccr4-Caf1 Deadenylase Complex in Nuclear Cajal Bodies. *Mol. Cell. Biol.*, **27**, 1686–1695.

14. Chen,H., Li,N., Xu,Y., Li,G., Song,C., Yao,R., Yu,T., Wang,J. and Yang,L. (2022) Novel compound heterozygous variant of TOE1 results in a mild type of pontocerebellar hypoplasia type 7: an expansion of the clinical phenotype. *neurogenetics*, **23**, 11–17.

15. Wang,C., Ge,Y., Li,R., He,G. and Lin,Y. (2023) Novel compound heterozygous missense variants in TOE1 gene associated with pontocerebellar hypoplasia type 7. *Gene*, **862**, 147250.

16. Wei,T., Shan,S., Jia,Z. and Ding,Y. (2024) Case report: A severe clinical phenotype of pontocerebellar hypoplasia type 7 with compound heterozygous variants of TOE1. *Heliyon*, **10**, e28678.

17. Kuroda,Y., Naruto,T., Tsuyusaki,Y., Kato,A., Aida,N. and Kurosawa,K. (2024) Role of TOE1 variants at the nuclear localization motif in pontocerebellar hypoplasia 7. *J. Hum. Genet.*, **69**, 349–355.

18. Kukulka,N.A., Singh,S., Whitehead,M.T., Dobyns,W.B., Chang,T. and Kousa,Y.A. (2025) Pontocerebellar hypoplasia: a review from 1912 to 2022. *Brain Commun.*, **7**, fcaf298.

19. Abramson,J., Adler,J., Dunger,J., Evans,R., Green,T., Pritzel,A., Ronneberger,O., Willmore,L., Ballard,A.J., Bambrick,J., *et al.* (2024) Accurate structure prediction of biomolecular interactions with AlphaFold 3. *Nature*, **630**, 493–500.

20. Sperandio,S., Barat,C., Cabrita,M.A., Gargaun,A., Berezovski,M.V., Tremblay,M.J. and De Belle,I. (2015) TOE1 is an inhibitor of HIV-1 replication with cell-penetrating capability. *Proc. Natl. Acad. Sci.*, **112**.

21. De Belle,I., Wu,J.-X., Sperandio,S., Mercola,D. and Adamson,E.D. (2003) In Vivo Cloning and Characterization of a New Growth Suppressor Protein TOE1 as a Direct Target Gene of Egr1. *J. Biol. Chem.*, **278**, 14306–14312.

22. Schäfer,I.B., Rode,M., Bonneau,F., Schüssler,S. and Conti,E. (2014) The structure of the Pan2–Pan3 core complex reveals cross-talk between deadenylase and pseudokinase. *Nat. Struct. Mol. Biol.*, **21**, 591–598.

23. Raisch,T., Chang,C.-T., Levdansky,Y., Muthukumar,S., Raunser,S. and Valkov,E. (2019) Reconstitution of recombinant human CCR4-NOT reveals molecular insights into regulated deadenylation. *Nat. Commun.*, **10**, 3173.

24. Wolf,J., Valkov,E., Allen,M.D., Meineke,B., Gordiyenko,Y., McLaughlin,S.H., Olsen,T.M., Robinson,C.V., Bycroft,M., Stewart,M., *et al.* (2014) Structural basis for P an3 binding to P an2 and its function in MRNA recruitment and deadenylation. *EMBO J.*, **33**, 1514–1526.

25. Hall,T.M.T. (2005) Multiple modes of RNA recognition by zinc finger proteins. *Curr. Opin. Struct. Biol.*, **15**, 367–373.

26. Mirdita,M., Schütze,K., Moriwaki,Y., Heo,L., Ovchinnikov,S. and Steinegger,M. (2022) ColabFold: making protein folding accessible to all. *Nat. Methods*, **19**, 679–682.

27. Boczonadi,V., Müller,J.S., Pyle,A., Munkley,J., Dor,T., Quartararo,J., Ferrero,I., Karcagi,V., Giunta,M., Polvikoski,T., *et al.* (2014) EXOSC8 mutations alter mRNA metabolism and cause hypomyelination with spinal muscular atrophy and cerebellar hypoplasia. *Nat. Commun.*, **5**, 4287.

28. Burns,D.T., Donkervoort,S., Müller,J.S., Knierim,E., Bharucha-Goebel,D., Faqeih,E.A., Bell,S.K., AlFaifi,A.Y., Monies,D., Millan,F., *et al.* (2018) Variants in EXOSC9 Disrupt the RNA Exosome and Result in Cerebellar Atrophy with Spinal Motor Neuronopathy. *Am. J. Hum. Genet.*, **102**, 858–873.

29. Fasken,M.B., Losh,J.S., Leung,S.W., Brutus,S., Avin,B., Vaught,J.C., Potter-Birriel,J., Craig,T., Conn,G.L., Mills-Lujan,K., *et al.* (2017) Insight into the RNA Exosome Complex Through Modeling Pontocerebellar Hypoplasia Type 1b Disease Mutations in Yeast. *Genetics*, **205**, 221–237.

30. Fasken,M.B., Morton,D.J., Kuiper,E.G., Jones,S.K., Leung,S.W. and Corbett,A.H. (2020) The RNA Exosome and Human Disease. In LaCava,J., Vaňáčová,Š. (eds), *The Eukaryotic*

RNA Exosome, Methods in Molecular Biology. Springer New York, New York, NY, Vol. 2062, pp. 3–33.

31. Runnebohm,A.M., Wijeratne,H.R.S., Barron,M.P., Smith-Kinnaman,W.R., Rooney,J.D., Peck Justice,S.A., Cureton,L.A., Holland,A., Ghalei,H., Pelletier,S., *et al.* (2025) EXOSC3 S1-domain variants implicated in PCH1b alter RNA exosome cap subunit abundance and thermal stability disrupting rRNA processing and targeting of AU-rich mRNA. *BioRxiv Prepr. Serv. Biol.*, 10.1101/2025.05.31.657176.

32. Sekulovski,S., Devant,P., Panizza,S., Gogakos,T., Pitiriciu,A., Heitmeier,K., Ramsay,E.P., Barth,M., Schmidt,C., Tuschl,T., *et al.* (2021) Assembly defects of human tRNA splicing endonuclease contribute to impaired pre-tRNA processing in pontocerebellar hypoplasia. *Nat. Commun.*, **12**, 5610.

33. Yang,A., Kong,X., Wang,Q., Miao,R., Ma,H., Chu,A., Wang,Z., Lu,J., Liu,B., Mu,B., *et al.* (2025) Novel heterozygous missense variants in the TOE1 gene linked to pontocerebellar hypoplasia type 7. *Genes Dis.*, **12**, 101290.

34. Sperandio,S., Tardito,S., Surzycki,A., Latterich,M. and De Belle,I. (2009) TOE1 interacts with p53 to modulate its transactivation potential. *FEBS Lett.*, **583**, 2165–2170.

35. Fong,K., Li,Y., Wang,W., Ma,W., Li,K., Qi,R.Z., Liu,D., Songyang,Z. and Chen,J. (2013) Whole-genome screening identifies proteins localized to distinct nuclear bodies. *J. Cell Biol.*, **203**, 149–164.

36. Wu,M., Reuter,M., Lilie,H., Liu,Y., Wahle,E. and Song,H. (2005) Structural insight into poly(A) binding and catalytic mechanism of human PARN: Crystal structure of PARN. *EMBO J.*, **24**, 4082–4093.

37. Tang,T.T.L. and Passmore,L.A. (2019) Recognition of Poly(A) RNA through Its Intrinsic Helical Structure. *Cold Spring Harb. Symp. Quant. Biol.*, **84**, 21–30.

FIGURES AND FIGURES LEGENDS

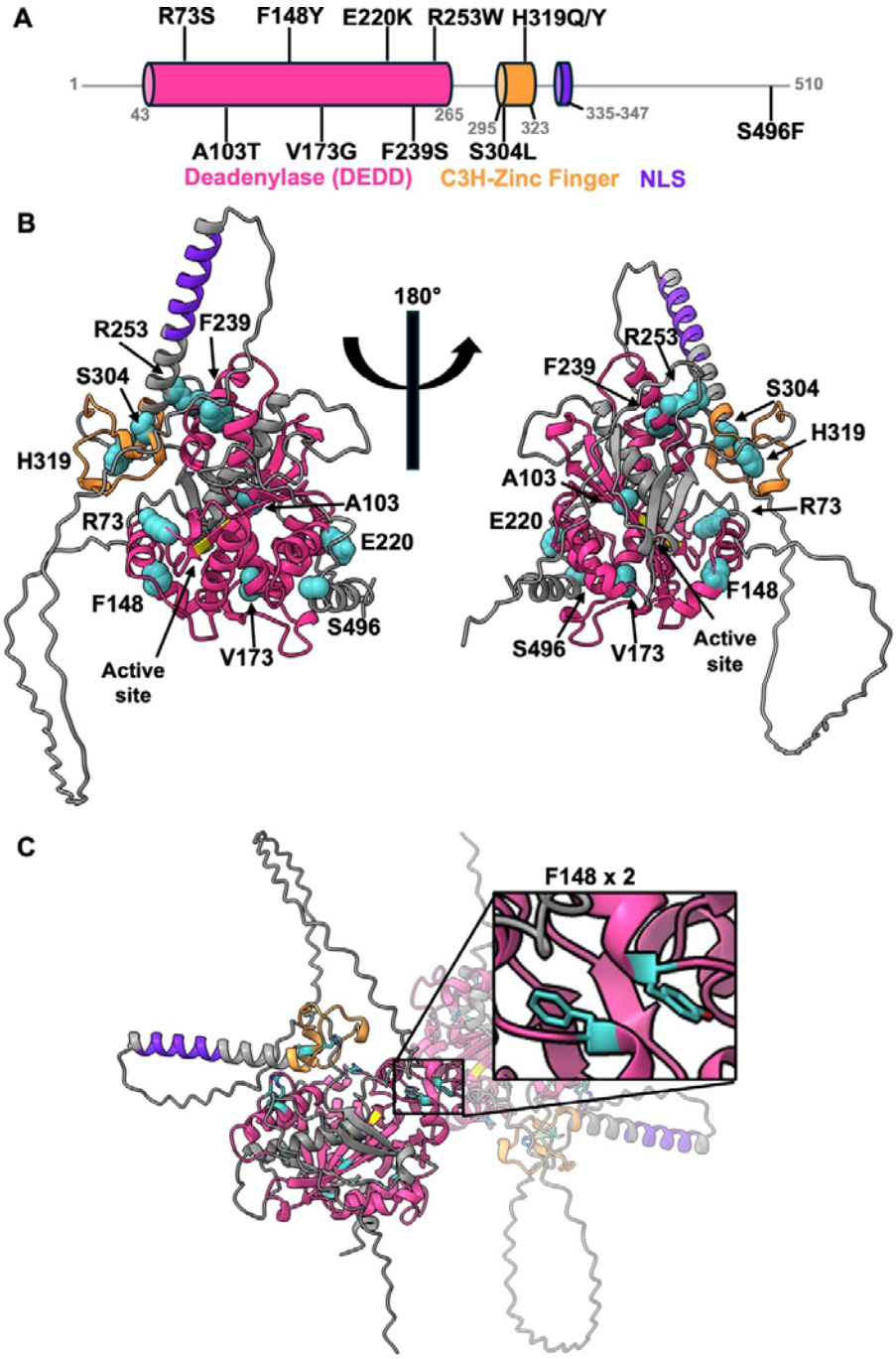

Figure 1: Architecture of TOE1 and location of PCH-variants.
A) The domain architecture of TOE1 labeled with the location of the PCH-linked mutations covered in this work. The deadenylase domain is colored in pink, the C3H zinc finger in orange, and the nuclear localization signal (NLS) in purple. PCH-linked variants are labeled in their respective location. B) An AlphaFold generated ribbon structure of the TOE1 monomer with PCH-linked TOE1 variants colored in a teal/cyan, with two active site (D64,E66) residues highlighted in yellow. C) An AlphaFold generated ribbon structure of homodimer of TOE1, with a zoom-in for the dimer interface with F148.

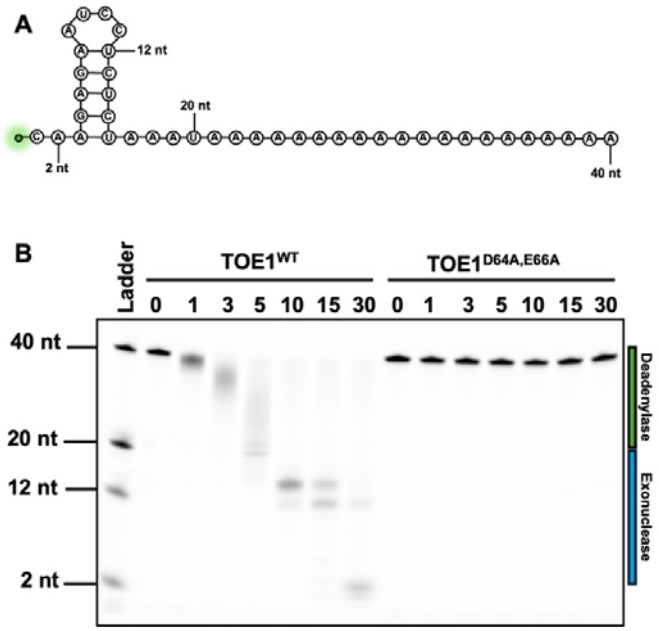

Figure 2: Recombinant TOE1^{WT} functions as a deadenylase and exonuclease.
A) The 5'- fluorescently labeled RNA substrate used in the ribonuclease assays contains a stem loop (CAAGAGAAUCCUCUCU), follow by AAAUA and a 20nt poly(A) tail(23). The regions where the RNA substrate sequence was truncated from the 3' end for the RNA ladder controls, is marked on this image. B) A representative 30-minute time course ribonuclease assay for TOE1^{WT} and TOE1^{D64A,E66A}. A green bar to the right of the gel notates the region of the gel that is deadenylase activity, while a blue bar indicates the region of exonuclease activity.

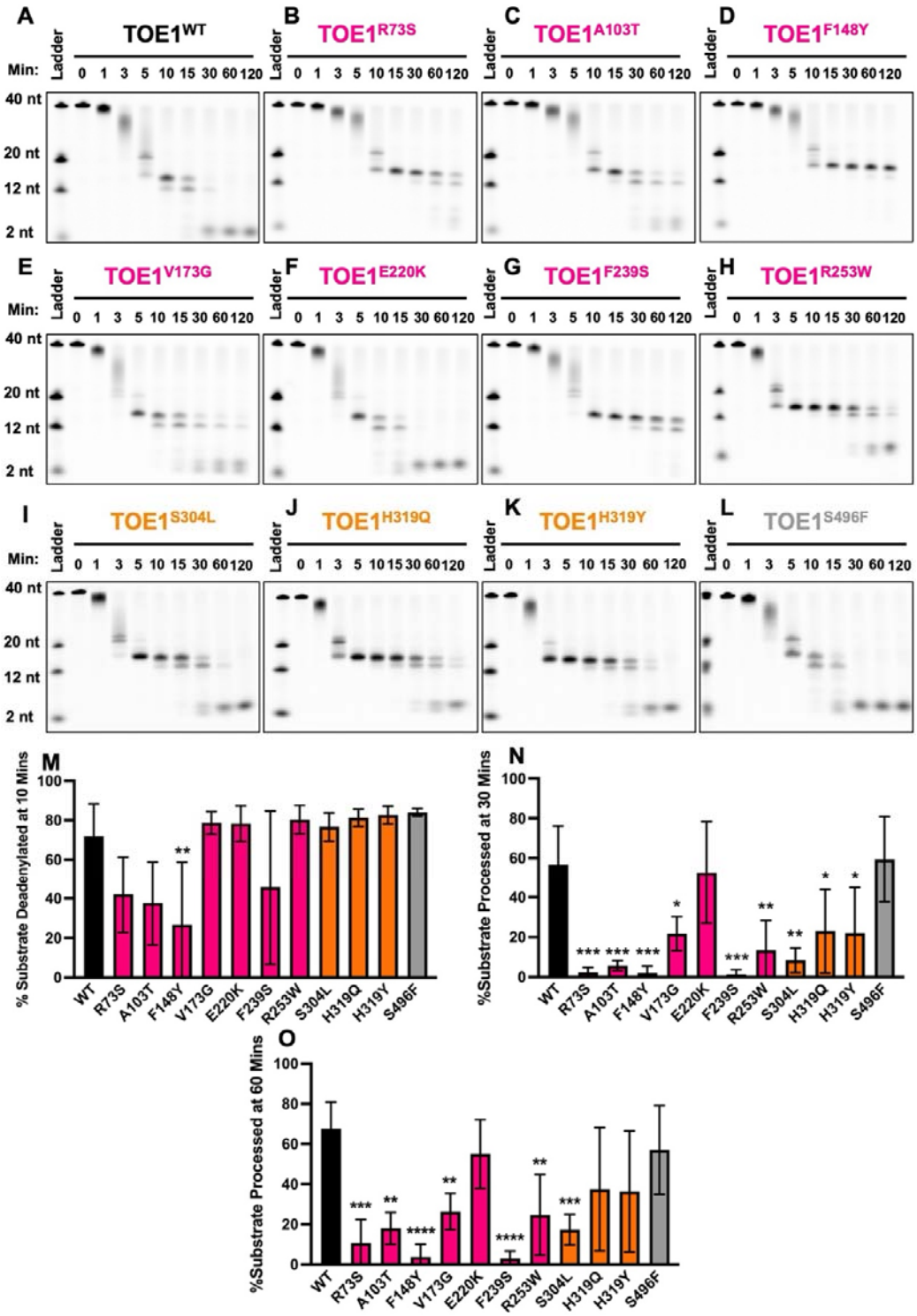

Figure 3: Ribonuclease assays reveal altered deadenylase and exonuclease functions for PCH-linked TOE1 variants. *TOE1 (250 nM) was assayed for cleavage of a 5'-fluorescently labeled RNA substrate (500 nM). A) WT, B) R73S, C) A103T, D) F148Y, E) V173G, F) E220K, G) F239S, H) R253W, I) S304L, J) H319Q, K) H319Y, and L) S496F. M) Mean percentage of deadenylated substrate after 10 minutes and N) Mean percentage of substrate fully processed in 30 minutes. O) Mean percentage of substrate fully processed in 60 minutes. *= p<0.05, **=p<0.01, ***=<0.001, ****=<0.0001 using a One-Way Anova.*

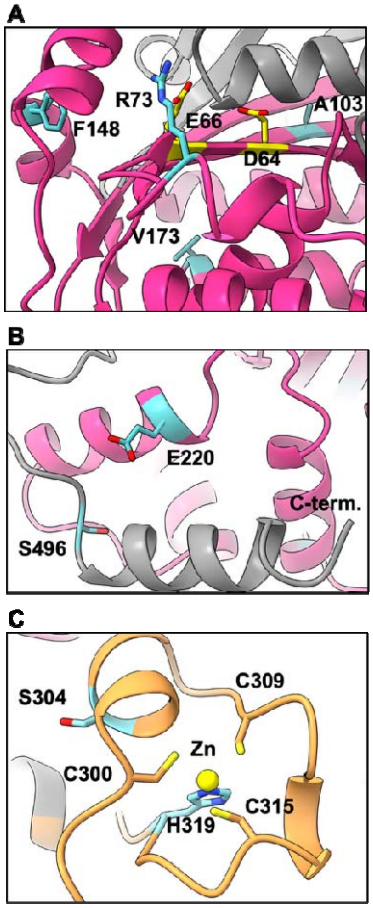

Figure 4: Structural predictions of TOE1 PCH mutations.
Structural depiction of the molecular environment of amino acids with PCH-linked variants that had notable ribonuclease activity. Amino acids with PCH-linked mutations, highlighted in this work, appear in teal/cyan. A) Most notable impacts were seen for R73, A103, and F148 for their impact on TOE1 deadenylase activity. The catalytic residues (D64, E66) are colored yellow. B) E220 and S496, which are located near the C-terminus of TOE1, were identified for having activity similar to wildtype. C) An AlphaFold 3 (19) generated TOE1 with a zinc ion (yellow) in the zinc finger domain (orange), coordinated by H319 and C300, C309, C315.

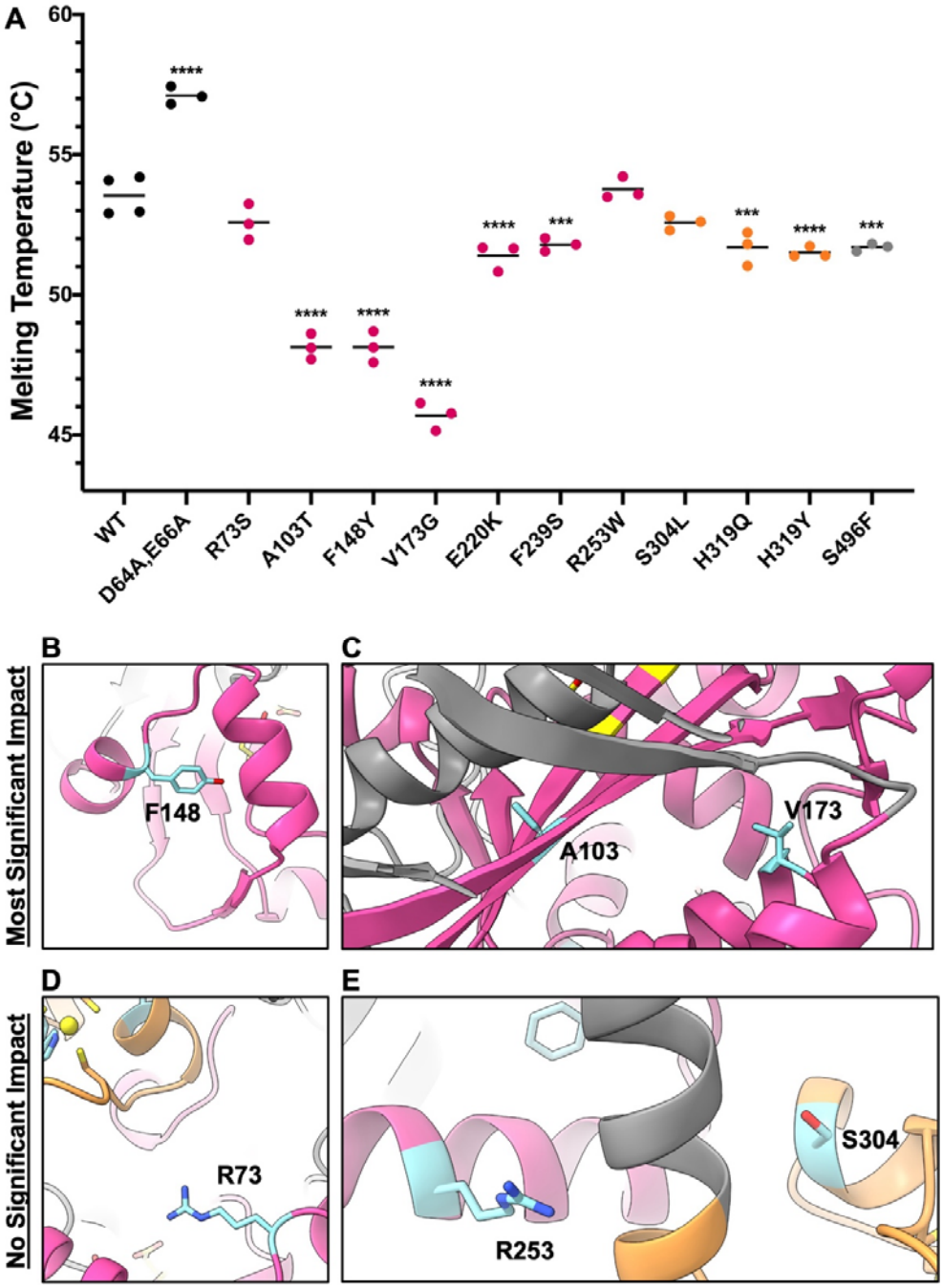

Figure 5: PCH mutations can impact the thermal stability of TOE1.
*A) Melting temperatures of TOE1 variants, calculated using DSF. Each point shown is an experimental replicate (unique protein purifications with assays on different days). Data was analyzed by one-way ANOVA (***= p<0.001 and **** =p< 0.0001). N=3 replicates, except for WT, for which N=4. B,C) The molecular environments of amino acids with variants that had the greatest impact on thermal stability F148, A103, and V173. D,E) The molecular environments of amino acids with variants that had no significant impact on thermal stability R73, R253, and S304. The amino acids with PCH-linked variants are shown in teal/cyan and are labeled.*

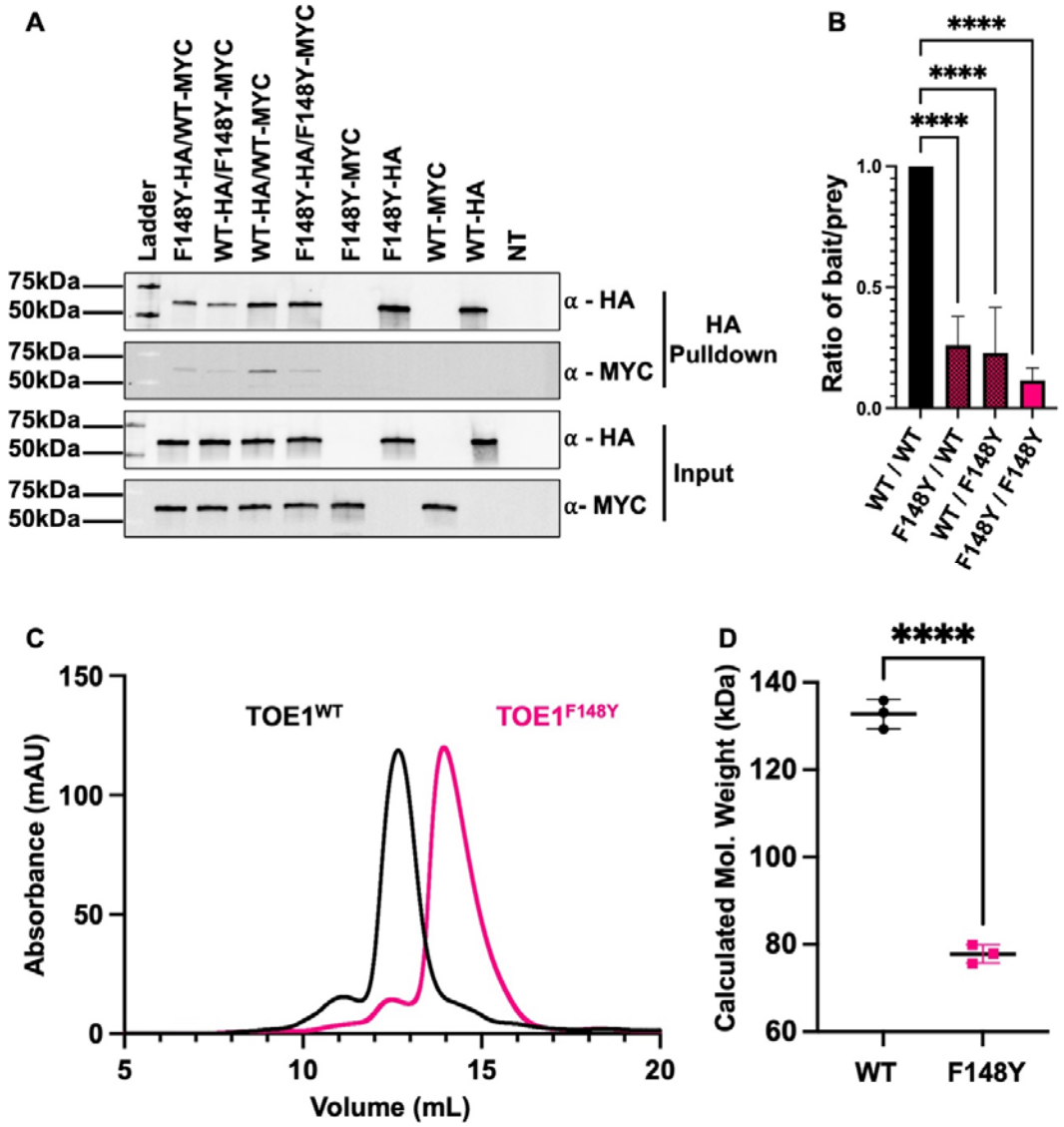

Figure 6: F148Y impairs TOE1 oligomerization

*A) Immunoprecipitation experiments of TOE1^{WT} and TOE1^{F148Y} tagged variants. B) The normalized ratio of the intensity of the bait TOE1 band/ intensity of the prey TOE1 band (N= 4)), normalized to the WT/WT ratio for each set of experiments. **** =p <0.0001 as analyzed by One-Way Anova. C) Size exclusion chromatography graph of TOE1^{WT} (black) and TOE1^{F148Y} (pink). D) Calculated molecular weight (MW) for TOE1^{WT} (black) and TOE1^{F148Y} (pink) done in replicate. **** =p <0.001 as analyzed by a Welch's t-test.*

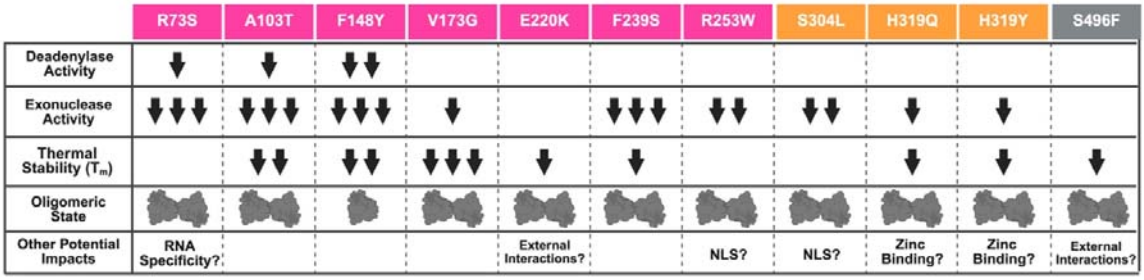

Figure 7: Summary of Biochemical Impacts of PCH-linked TOE1 Variants

Summary graphic of the impacts of PCH-lined TOE1 mutations on TOE1 deadenylation, exonuclease activity, stability, oligomerization, and other hypothesized impacts. Created in BioRender. Hayne, C. (2025) https://BioRender.com/7or78kz

SUPPLEMENTARY DATA

SUPPLEMENTARY TABLES

Supplemental Table 1: Plasmids Used in this work

Plasmid Backbone	Insert	Source
pHis2	WT D64A, E66A R73S A103T F148Y V173G E220K F239S R253W S304L H319Q H319Y S496F	Original cDNA synthesis/mutagenesis: Genscript Subcloning: In-house
pCDNA3.1	HA - TOE1	Genscript
	HA - TOE1 (F148Y)	Subcloned in house.
	MYC- TOE1	
	MYC- TOE1 (F148Y)	

Supplemental Table 2. Deadenylation and Exonuclease Completion of TOE1 Variants. *Calculated percentage of substrate deadenylated at 10 minutes or percentage of substrate degraded at 30 and 60 minutes for each reported PCH mutation. Replicates (N) are from individual protein preps. Standard deviation and p-value based on a One-Way Anova are reported.*

		Completed Deadenylation at 10 Minutes			Completed Exonuclease at 30 Minutes			Completed Exonuclease at 60 Minutes		
	N	**Mean (%)**	**Std. Dev.**	**p-value**	**Mean (%)**	**Std. Dev.**	**p-value**	**Mean (%)**	**Std. Dev.**	**p-value**
WT	10	71.90	16.41	N/A	56.50	19.62	N/A	67.70	13.24	N/A
R73S	3	42.00	19.29	0.124	2.33	2.52	0.0002	10.67	11.72	0.0002
A103T	3	37.67	21.20	0.0522	5.67	2.52	0.0006	18.00	7.94	0.0012
F148Y	3	26.67	32.13	0.0043	2.00	3.46	0.0002	3.67	6.35	<0.0001
V173G	3	78.67	5.69	0.9996	21.67	8.51	0.0316	26.33	9.07	0.0091
E220K	3	78.33	9.02	0.9997	52.67	25.74	>0.9999	55.00	17.09	0.9396
F239S	3	45.67	39.02	0.2383	1.33	2.31	0.0002	3.00	3.61	<0.0001
R253W	3	80.33	7.23	0.9972	13.33	14.98	0.0042	24.67	20.03	0.0061
S304L	3	76.67	7.23	>0.9999	8.33	6.11	0.0012	17.33	7.64	0.001
H319Q	4	81.25	4.35	0.9857	23.00	20.94	0.0179	37.50	30.83	0.0529
H319Y	3	82.67	4.51	0.9817	22.00	22.91	0.0341	36.33	30.14	0.0842
S496F	3	84.00	2.00	0.9597	59.33	21.55	>0.9999	57.00	22.11	0.9803

Supplemental Table 3. Summary Table of Thermal Stability Data.
Calculated Thermal for each PCH mutation. Replicates (N) are from individual protein preps. Standard deviation and p-value based on a One-Way Anova are reported.

	Mean T_m (°C)	Std. Dev. (°C)	N	p-value
WT	53.54	0.700	4	N/A
D64A,E66A	57.11	0.316	3	<0.0001
R73S	52.58	0.642	3	0.1014
A103T	48.14	0.456	3	<0.0001
F148Y	48.14	0.555	3	<0.0001
V173G	45.69	0.500	3	<0.0001
E220K	51.39	0.485	3	<0.0001
F239S	51.79	0.235	3	0.0004
R253W	53.77	0.396	3	0.9987
S304L	52.57	0.257	3	0.0956
H319Q	51.69	0.605	3	0.0002
H319Y	51.51	0.199	3	<0.0001
S496F	51.70	0.137	3	0.0002

SUPPLEMENTARY FIGURES

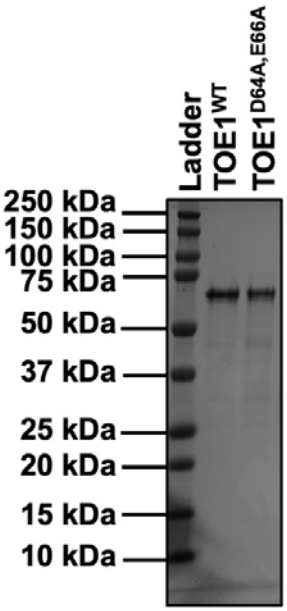

Supplemental Figure 1: Purification of recombinant TOE1. *Representative SDS-PAGE gel of purified TOE1^{WT} and TOE1^{D64A,E66A}.*

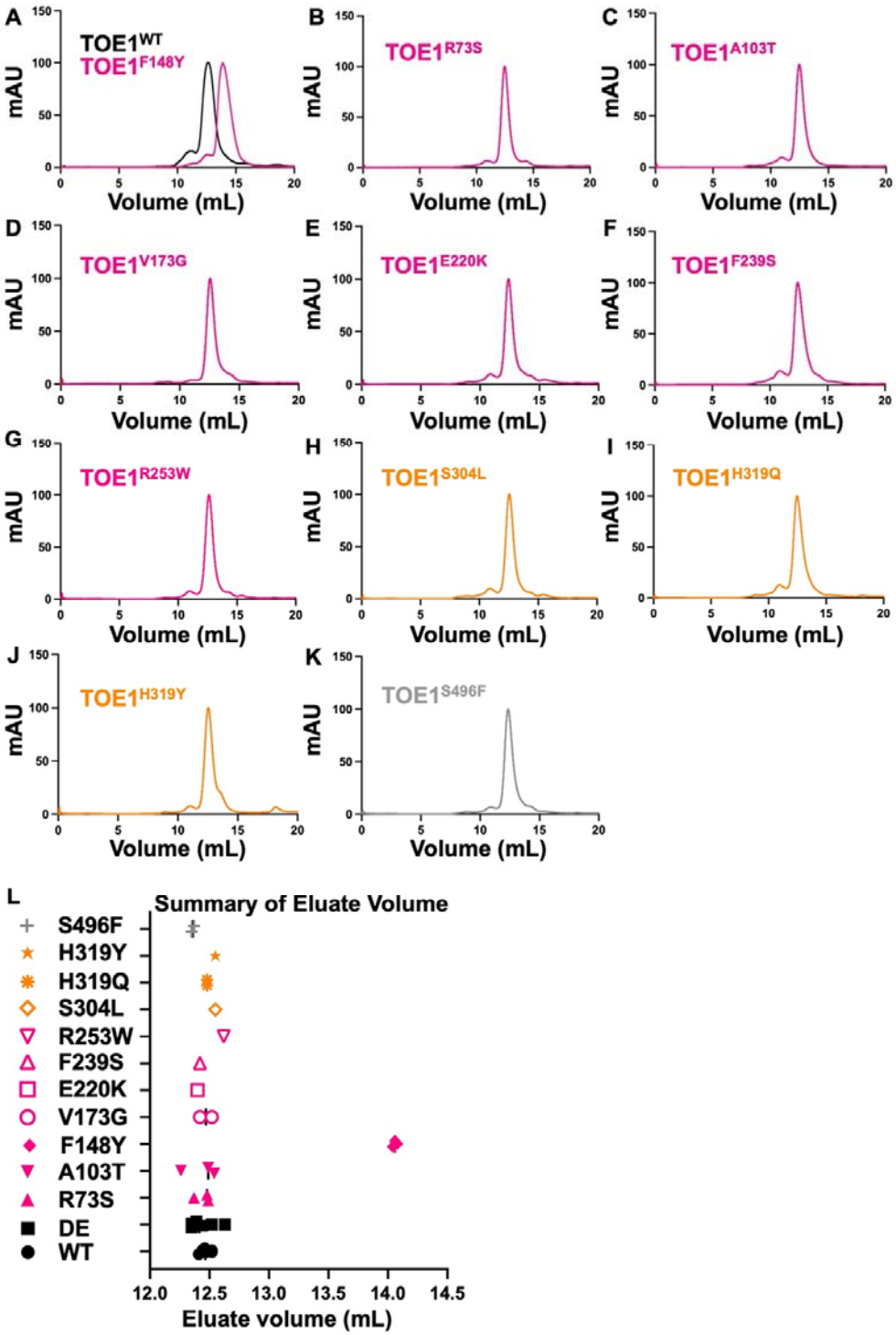

Supplemental Figure 2: S200 gel filtration traces for PCH7-linked TOE1 variants. *Profiles of size exclusion chromatographs, normalized to the highest absorbance for each run. A) F148Y and WT replicate, B) R73S C) A103T, D) V173G, E) E200K, F) F239S, G) R253W, H) S304L, I) H319Q, J) H319Y, K) S496F, L) Summary of the peak eluate volume for each PCH7-variant measurement.*

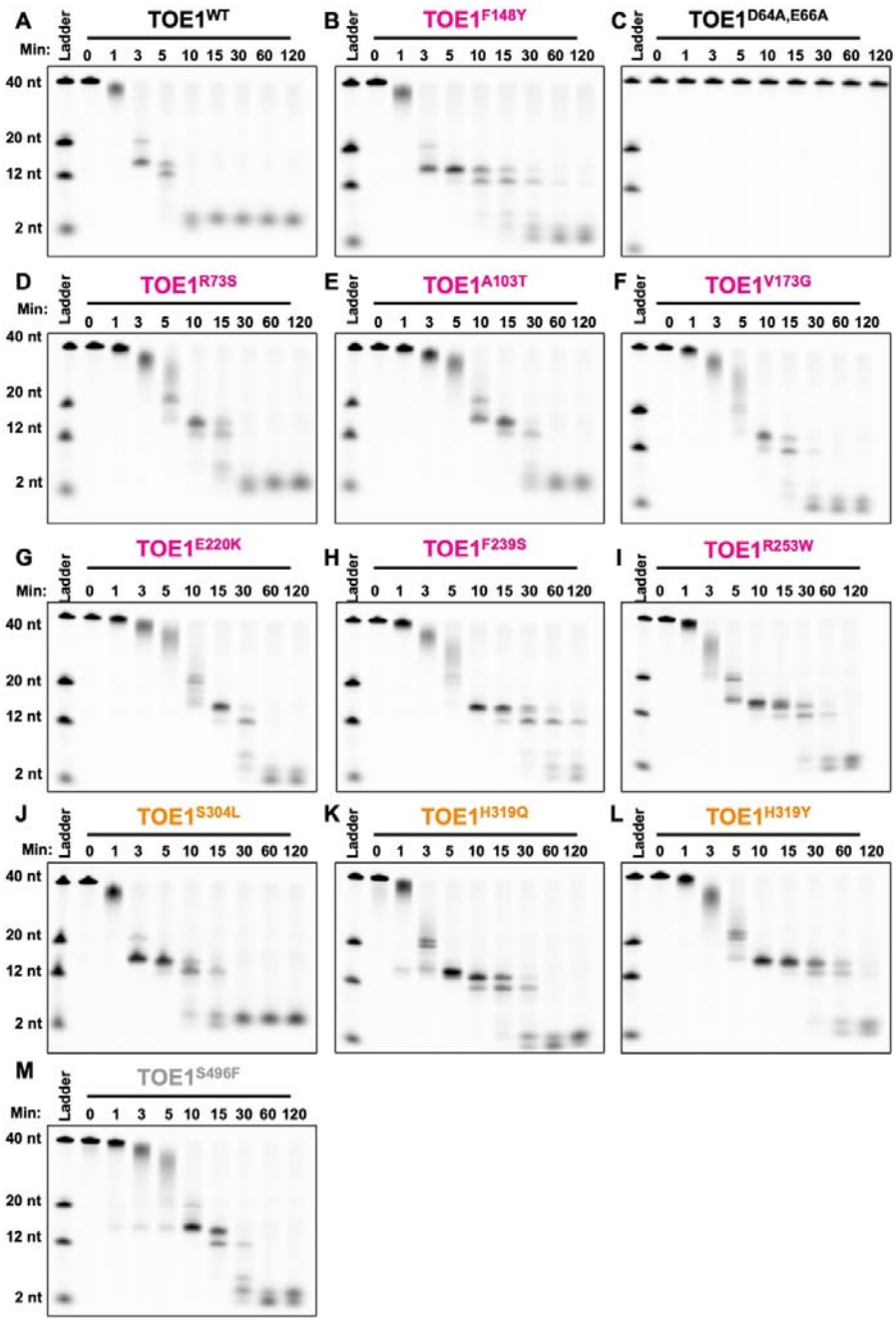

Supplemental Figure 3: Ribonuclease assays of eluates from the gel filtration for tested variants. *TOE1 (250 nM) was assayed for cleavage of 5'-fluorescently labeled RNA substrate (500 nM). A) WT, B) F148Y, C) D64A,E66A, D), E) R73S, F) A103T, G) V173G, H) E220K, I) R253W, J) S304L, K) H319Q, L) H319Y. and M) S496F.*